frontiers | Frontiers in Chemistry

TYPE Original Research
PUBLISHED 19 October 2022
DOI 10.3389/fchem.2022.962528

OPEN ACCESS

EDITED BY
Qingzhi Wu,
Wuhan University of Technology, China

REVIEWED BY
Xuanbo Zhu,
Jilin University, China
Zhubing Xiao,
Henan University, China

*CORRESPONDENCE
Zhengshan Tian,
tianzhengshan@163.com
Suzhen Bai,
szb0211@163.com

SPECIALTY SECTION
This article was submitted to Inorganic Chemistry,
a section of the journal
Frontiers in Chemistry

RECEIVED 06 June 2022
ACCEPTED 04 October 2022
PUBLISHED 19 October 2022

CITATION
Tian Z, Tian H, Cao K, Bai S, Peng Q, Wang Y and Zhu Q (2022), Facile preparation of $Ti_3C_2T_x$ sheets by selectively etching in a H_2SO_4/H_2O_2 mixture.
Front. Chem. 10:962528.
doi: 10.3389/fchem.2022.962528

Facile preparation of $Ti_3C_2T_x$ sheets by selectively etching in a H_2SO_4/H_2O_2 mixture

Zhengshan Tian[1]*, Hao Tian[2], Kesheng Cao[1], Suzhen Bai[1]*, Qinlong Peng[1], Yabo Wang[1] and Qiuxiang Zhu[3]

[1]School of Chemistry and Environmental Engineering, Henan Key Laboratory of Germplasm Innovation and Utilization of Eco-economic Woody Plant, Pingdingshan University, Pingdingshan, China, [2]School of Pharmacy, Henan University of Chinese Medicine, Zhengzhou, China, [3]College of Information and Electronic Engineering, Hunan City University, Yiyang, China

MXenes and MXene-based composite materials have potential applications in a wide range of areas due to their unique physical and chemical characteristics. At present, it is still a major challenge to develop a simple, safe, and efficient route to prepare MXenes without using fluorinated etchants. Herein, we design a facile method to prepare $Ti_3C_2T_x$ MXene sheets by selectively etching Ti_3AlC_2 powders in an aqueous diluted H_2SO_4 solution with H_2O_2 as an oxidant. In a system of H_2SO_4 and H_2O_2, an aqueous H_2SO_4 solution with a concentration of 6 mol/L is a strongly acidic medium with no volatility, and 30% H_2O_2 acts as a strong green oxidizer without harmful by-products. The experimental process is safe and convenient to conduct in a beaker under a water bath of 40°C. The etching process can be completed in 1 h under the air atmosphere conditions. The experimental results confirmed that the etched Ti_3AlC_2 powders can be successfully separated into $Ti_3C_2T_x$ nanosheets under ultrasound treatment without using any intercalation agent. The relevant etching mechanism is may be attributed to the synergy effect of H_2SO_4 and H_2O_2, which triggers sequential selective etching of Al layers from the Ti_3AlC_2 phase. It may provide a new green way to prepare MXene-based materials without using toxic HF or HF-containing etchants.

KEYWORDS

Ti_3AlC_2 powders, $Ti_3C_2T_x$ sheets, H_2SO_4/H_2O_2 mixture, selective etching, HF-containing etchants

Introduction

Since a new family of two-dimensional (2D) materials was first discovered in 2011 (Naguib et al., 2011), increasing attention has been paid to these novel 2D transition metal carbides, carbonitrides, and nitrides (named MXenes), and currently, more than 40 MXene compositions (Naguib et al., 2021) have been synthesized by different efficient routes (Naguib and Gogotsi, 2015; Alhabeb et al., 2017; Anasori et al., 2017; Tao et al., 2017; Zhou et al., 2017; Gogotsi and Anasori, 2019; Fan et al., 2022). The MAX phases are layered ternary carbides and nitrides with a general formula $M_{n+1}AX_n$, where M represents transition metals (such as Sc, Ti, Zr, Hf, V, Nb, Ta, Cr, Mo, etc.), A

represents elements from the group 13 and 14 of the periodic table, and X is carbon and/or nitrogen (Naguib and Gogotsi, 2015). After the discovery of $Ti_3C_2T_x$ MXene in 2011 (Naguib et al., 2011), many MXenes were synthesized by selectively etching different precursors in liquid mediums such as HF, HF-containing, or HF-forming etchants; thus, these etching processes unavoidably caused some surface functional groups such as −O, −F, or −OH, marked as T_x in a general formula $M_{n+1}X_nT_x$ for MXenes (Naguib and Gogotsi, 2015; Anasori et al., 2017; Tao et al., 2017; Zhou et al., 2017).

More importantly, MXenes and MXene-based composite materials have potential applications in various fields such as energy storage (Lukatskaya et al., 2013; Ghidiu et al., 2014; Liang et al., 2015; Wang et al., 2015; Luo et al., 2020; VahidMohammadi et al., 2021), flexible electronics (Xu et al., 2021a; Xu et al., 2021b; Shi et al., 2022a; Xu et al., 2022), electromagnetic shielding (Shahzad et al., 2016; Iqbal et al., 2020), catalysis (Seh et al., 2016; Liu et al., 2020), and water treatment (Ren et al., 2015) due to their unique physical and chemical properties (Halim et al., 2014; Dillon et al., 2016; Hantanasirisakul et al., 2016). In order to promote their potential applications, numerous research efforts have been carried out to explore the emerging etching methods and the stable storage of MXene, especially the large-scale preparing methods (Naguib and Gogotsi, 2015; Alhabeb et al., 2017; Gogotsi and Anasori, 2019; Fan et al., 2022).

In general, MXene nanosheets were synthesized by selectively etching MAX phases, as well as subsequent intercalation and delamination. In the early stage, the typical etching methods were dominated by HF etching methods (Naguib et al., 2011) and *in situ* HF-forming etching methods (Ghidiu et al., 2014; Halim et al., 2014). For example, Gogotsi et al. designed that the synthesis of MXene can be scaled up in a small-batch wet chemical etching process, and 1.0 g of the Ti_3AlC_2 powders was slowly peeled off in a system of HF and HCl for 24 h at 35°C (Shuck et al., 2020). Since 2017, fluorine-free etching methods such as electrochemical etching methods (Pang et al., 2019), alkali etching methods (Li et al., 2017; Li et al., 2018), molten salt etching methods (Li et al., 2019), halogen etching methods (Jawaid et al., 2021; Shi et al., 2021), and other methods (Ghazaly et al., 2021) were developed to prepare fluorine-free MXenes with different characteristics. For example, the electrochemical etching method (Pang et al., 2019) and alkali etching method (Li et al., 2018) can avoid the use of fluorinated etchants, and at the same time, the HF toxicity to the human body, corrosiveness, and harm to the environment can be effectively avoided. In 2019, a new method for MAX phase etching at a high temperature of 550°C was developed by using Lewis acid molten salt as an etching agent (Li et al., 2019). This method avoids the use of HF, HF-containing, or HF-forming etchants, but the high temperature is a necessary condition. In 2021, Song et al. developed a controllable HCl-hydrothermal etching strategy for Mo_2CT_x MXenes based on DFT calculation (Wang et al., 2021). In this process, Mo_2CT_x MXenes were prepared through a hydrothermal etching process with concentrated HCl in an autoclave at 120 or 140°C for 5 days. However, the high concentration, high temperature, and long etching time also impede its widespread use. More recently, Xiao et al. delicately exploited a low-temperature photo-Fenton strategy to fabricate F-free Ti_3C_2 with 95% high purity, and this work would play an important role in the F-free fabrication of MXene and synthesis of cathodes with excellent performance for flexible lithium-sulfur batteries (Liang et al., 2022).

In addition, the intercalation and delamination strategies of MXenes are mainly divided into organic intercalator delamination, inorganic intercalator delamination, and mechanical delamination (Mashtalir et al., 2013; Sang et al., 2016). The principle of intercalation and delamination is based on weakening the interlayer force (such as hydrogen bonding and van der Waals forces) among MXene nanosheets (Naguib et al., 2011; Alhabeb et al., 2017).

Although many successful synthetic routes and delamination routes of MXenes have been reported in the literature (Naguib et al., 2011; Alhabeb et al., 2017; Gogotsi and Anasori, 2019; Naguib et al., 2021; Fan et al., 2022), there are still a number of disadvantages such as the corrosion of etching agent to experimental equipment, harmful impact of reagents on the environment, and severe operating conditions. Therefore, it is highly desirable to develop a simple, safe, and efficient protocol for the synthesis of MXenes, and it is still a major challenge.

Inspired by the synthesis of MXenes through a controllable HCl-hydrothermal etching (Wang et al., 2021), a selective etching of MAX phase (Ti_3SiC_2) by using a solution of HF with oxidant (such as H_2O_2) (Alhabeb et al., 2018) and highly reactive radicals ($HO^{\bullet}$ and $O_2^{\bullet-}$) weakening the Ti–Al bonds in the MAX phase (Liang et al., 2022), we design a facile method to produce $Ti_3C_2T_x$ MXenes by etching Ti_3AlC_2 powders in a system of H_2SO_4 and H_2O_2. In this system, an aqueous dilute H_2SO_4 solution is not volatile nor toxic, and H_2O_2 is a green oxidant; thus, this experimental process is safe and convenient to conduct in a beaker. The experimental results confirmed that $Ti_3C_2T_x$ nanosheets can be successfully obtained, and this method is safe, rapid, and efficient.

Experimental section

Materials

Ti_3AlC_2 powders (98 wt% purity, 200 mesh) were purchased from Shanghai Rohn Reagent Co., Ltd. Sulfuric acid (H_2SO_4, 18 mol/L), hydrogen peroxide (H_2O_2, 30%), and sodium hydroxide (NaOH, analytical grade) were purchased from the National Pharmaceutical Reagent Company. All chemicals were used without further purification. Deionized water (a resistance

of 18 MΩ) made from a Milli-Q solvent system was used throughout all the experiments.

Preparation of $Ti_3C_2T_x$ Sheets

As a typical MAX phase, Ti_3AlC_2 powders were selected to be etched in a mixture of H_2SO_4 and H_2O_2 in our experiment.

1) Al layer etching. Typically, 2.0 g of Ti_3AlC_2 powders and 50 ml of H_2SO_4 solution (6 mol/L) were added into a beaker (200 ml) under electromagnetic stirring conditions. Then, 20 ml of H_2O_2 (30%) was slowly dropped into the abovementioned dispersion within 30 min under electromagnetic stirring conditions. A temperature-controlled water pot was used to control the temperature of 40 °C for this etching. Next, the obtained dispersion was still stirred at 40 °C for 30 min to further etch the Al layers from the Ti_3AlC_2 phase.
2) Sediment cleaning. After etching Al layers, the obtained dispersion was centrifuged at 3,000 rpm for 10 min with a high-speed centrifuge (Neofuge1600R) to obtain the sediment and recycle supernatant (including the etched Al layers and H_2SO_4 solution), respectively. The obtained sediment was cleaned with deionized water several times until the pH of the dispersion was close to 7. In addition, a nanocomposite of Al_2O_3 and TiO_2 can be obtained from the supernatant by adding an appropriate amount of NaOH solution.
3) Ultrasonic stripping. A small amount of the obtained sediment was taken out and placed in a beaker with deionized water. No intercalation agent was required in this process. An ultrasonic cleaner was used to separate the obtained sediment in the beaker for 20 min to prepare $Ti_3C_2T_x$ sheets with appropriate ultrasonic power (KQ-300GDV, frequency 40 kHz, output power 300 W, 50% amplitude). After ultrasonic treatment, the obtained aqueous solution of MXenes was filtered through a mixed cellulose ester microporous membrane using a water-circulating multi-purpose vacuum pump (SHB-III). Finally, the obtained sample was dried in a vacuum at 60°C for 24 h for characterizations.

Characterizations

The microstructure of Ti_3AlC_2 powders and $Ti_3C_2T_x$ sheets were detected by scanning electron microscopy (SEM, Hitachi S-4800) and transmission electron microscopy (TEM, JEM-2100). The X-ray diffractometer (XRD, Bruker D8 diffractometer), Fourier transform infrared spectroscopy (FTIR, Nicolet5700), and X-ray photoelectron spectroscopy (XPS, K-alpha1063) were used to analyze the etching process and the relevant etching mechanism of Ti_3AlC_2 powders.

Results and discussion

Structure analysis

Based on the synthetic strategies of HCl-hydrothermal etching (Wang et al., 2021), HF/H_2O_2 oxidant-assisted etching (Alhabeb et al., 2018), and photo-Fenton radicals weakening, (Liang et al., 2022) a facile, safe, and rapid strategy was designed to prepare $Ti_3C_2T_x$ MXenes by selectively etching Ti_3AlC_2 powders in an aqueous H_2SO_4 solution with H_2O_2 as oxidant. The detailed preparation process (including etching, cleaning, and stripping) was introduced in the experimental section, and the schematic procedure is shown in Figure 1A. The mixture of Ti_3AlC_2 powders and aqueous H_2SO_4 solution is black (Figure 1B), while an aqueous solution of $Ti_3C_2T_x$ sheets without cleaning and stripping has a purple/magenta color (Naguib et al., 2011), as shown in Figure 1C. After cleaning and stripping, the resulting aqueous solution of $Ti_3C_2T_x$ nanosheets presents a shallow green color (Figure 1D). Both the aqueous solutions have clear Tyndall effects under natural light (Li et al., 2017), indicating the presence of $Ti_3C_2T_x$ nanosheets in two aqueous solutions, as shown in Figures 1C,D. Moreover, the resulting aqueous solution of $Ti_3C_2T_x$ nanosheets can be kept for 90 days under the low temperature of 1–4°C without any color change.

In order to explore the etching effect, SEM images of the Ti_3AlC_2 powders and the obtained $Ti_3C_2T_x$ sheets are carried out as contrast experiments. Figure 2 shows the microstructure of the Ti_3AlC_2 powders with different magnifications. It can be seen that the morphology and size of the Ti_3AlC_2 powders are very irregular (Figure 2B), and the individual particle has a compact layered structure, as shown in Figures 2C,D.

In contrast, SEM images in Figure 3 show the structural morphology of the obtained $Ti_3C_2T_x$ sheets. The color of the obtained $Ti_3C_2T_x$ MXene sheets is different from that of the Ti_3AlC_2 powders, namely, the colors change from black (Figure 2A) of the Ti_3AlC_2 powders to dark gray of the MXene sheets (Figure 3A). More importantly, the layered structure of the obtained $Ti_3C_2T_x$ sheets is notably different from that of the Ti_3AlC_2 powders (Figures 2B–D), as clearly demonstrated in Figures 3B–D. Particularly, the structure of the obtained $Ti_3C_2T_x$ sheets has some layered changes, and the lamellae have many hole defects, compared with that of the Ti_3AlC_2 powders; it is reasoned that when Al layers are etched away, a small amount of Ti layers is also etched out to leave holes and TiO_2 nanoparticles on the surfaces due to the Ti vacancies triggering the oxidation process from Ti to TiO_2, consistent with the results previous literature reported (Shi et al., 2022b; Huang et al., 2022; Jiang et al., 2022; Ma et al., 2022; Zhang et al., 2022).

To further demonstrate the morphology of $Ti_3C_2T_x$ sheets, TEM imaging was performed after the obtained $Ti_3C_2T_x$ sheets were treated by ultrasonic stripping in deionized water for 20 min. As shown in Figure 4, the obtained $Ti_3C_2T_x$

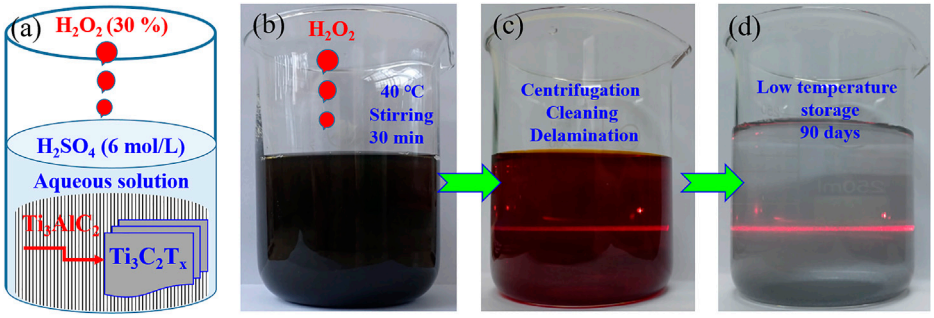

FIGURE 1
$Ti_3C_2T_x$ nanosheets prepared by selective etching in a system of H_2SO_4 and H_2O_2. Schematic illustration of a preparation procedure in a beaker **(A)**. Digital photographs of a mixture of Ti_3AlC_2 powders and aqueous H_2SO_4 solution **(B)**, aqueous MXenes solution after Al layers etching **(C)**, and aqueous MXenes solution after delamination **(D)**.

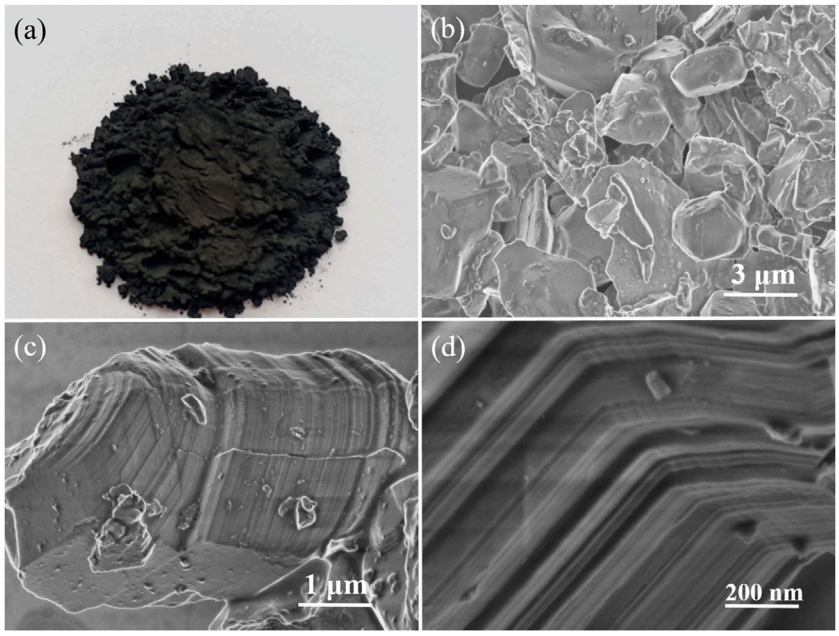

FIGURE 2
Digital photograph of the Ti_3AlC_2 powders **(A)**, SEM images of the Ti_3AlC_2 powders with different magnifications **(B–C)**, and magnified section SEM image of individual particle of Ti_3AlC_2 powders **(D)**.

nanosheets are single-layer or multilayer sheets with folded structures, consistent with the reported literature (Huang et al., 2022; Ma et al., 2022). A slight amount of TiO_2 nanoparticles on the MXene surface can be ascribed to the Ti vacancies triggering the oxidation process from Ti to TiO_2, consistent with SEM images in Figures 3B–D. Thus, the Ti_3AlC_2 powders can be easily stripped into $Ti_3C_2T_x$ nanosheets by a simple oxidative etching and subsequent ultrasonic exfoliation in our experiments.

In order to analyze the etching process, the XRD patterns and FTIR spectra of the Ti_3AlC_2 powders and the $Ti_3C_2T_x$ sheets were used to monitor their structural changes. From the distribution of the XRD peaks in Figure 5A, the Ti_3AlC_2 powders and $Ti_3C_2T_x$ sheets have characteristic peaks at different positions, such as (002), (004), (101), (104), (105), and so on (Naguib et al., 2011; Alhabeb et al., 2017; Li et al., 2017; Li et al., 2018; Li et al., 2019). In particular, the XRD (002) peak of the $Ti_3C_2T_x$ sheets is shifted toward a lower angle, namely, the peaks change from 9.75° of

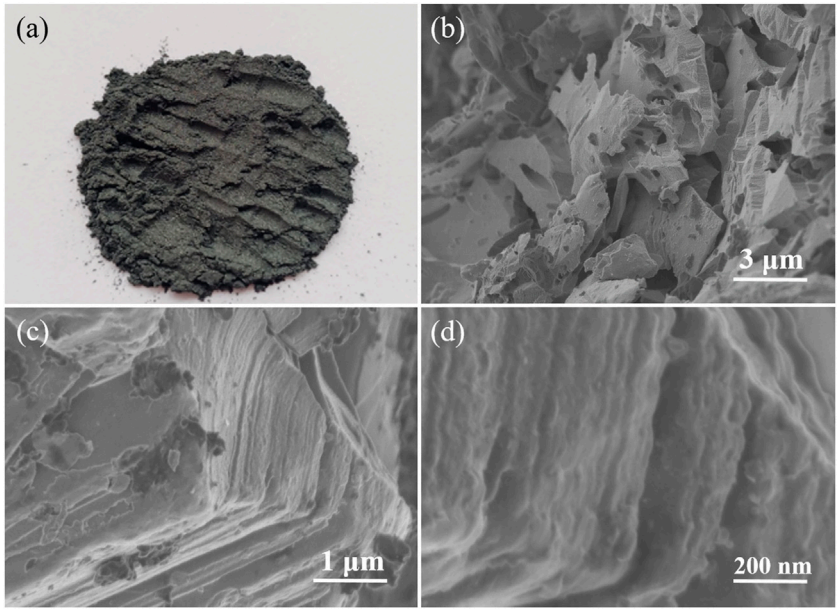

FIGURE 3
Digital photograph of $Ti_3C_2T_x$ sheets **(A)**, SEM images of $Ti_3C_2T_x$ sheets obtained by etching Ti_3AlC_2 powders in the H_2SO_4/H_2O_2 solution with different magnifications **(B–C)**, and magnified cross-section SEM image of $Ti_3C_2T_x$ sheets **(D)**.

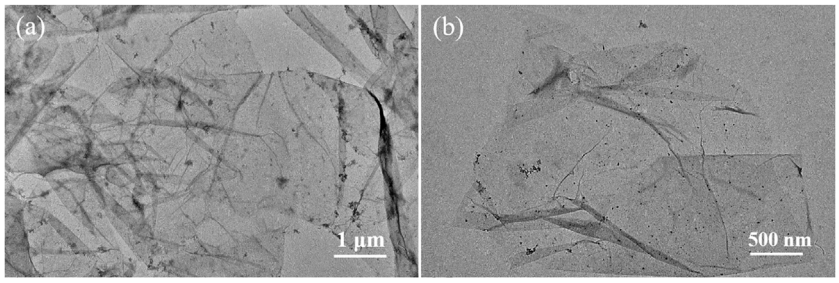

FIGURE 4
TEM images of $Ti_3C_2T_x$ nanosheets with different magnifications **(A)** and **(B)**.

Ti_3AlC_2 powders to 9.30° of $Ti_3C_2T_x$ sheets, indicating a larger spacing caused by etching Al atoms. Moreover, a certain amount of Ti_3AlC_2 is probably still present in $Ti_3C_2T_x$. From the FTIR spectra in Figure 5B, some new peaks appear, and they are very different from that of the pristine Ti_3AlC_2 powders. It can be found that there are lots of surface functional groups (Gao et al., 2021) such as 3,430 cm^{-1} of -OH, 1,620 cm^{-1} assigned to C=O, 1,400 cm^{-1} to the hydrogen bond of O-H, 1,090 cm^{-1} of C-O-C vibration, 790 cm^{-1} of the Ti-O bond (Wang et al., 2017), 610 cm^{-1} of SO_4^{2-} vibration (Lin, 2015), and 460 cm^{-1} of Ti-C vibration (Wang et al., 2017). Thus, these new peaks of the FTIR spectrum may be attributed to the oxidation of H_2O_2 and the intercalation of SO_4^{2-} (Lin, 2015; Wang et al., 2017; Gao et al., 2021).

In order to further explore the oxidation etching process, the XPS analysis of Ti_3AlC_2 powders and $Ti_3C_2T_x$ sheets were performed to reveal their changes in chemical compositions. It can be found that the XPS survey spectra of $Ti_3C_2T_x$ sheets present some new changes, such as a new peak of S 2p and a relatively elevated ratio of O 1s peak to C 1s peak (Figure 6A), compared with that of Ti_3AlC_2 powders.

Moreover, the high-resolution S 2p XPS analysis (Figure 6B) confirms that the new peak (Park and Leitao, 2021) of S 2p is attributed to SO_4^{2-}, consistent with the abovementioned FTIR

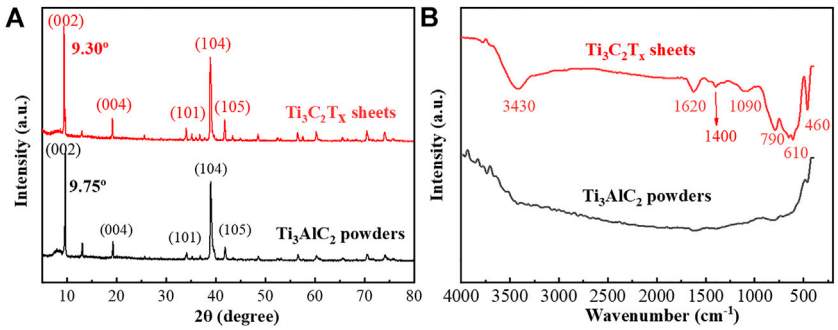

FIGURE 5
XRD patterns of Ti_3AlC_2 powders and $Ti_3C_2T_x$ sheets **(A)**, and FTIR spectra of Ti_3AlC_2 powders and $Ti_3C_2T_x$ sheets **(B)**.

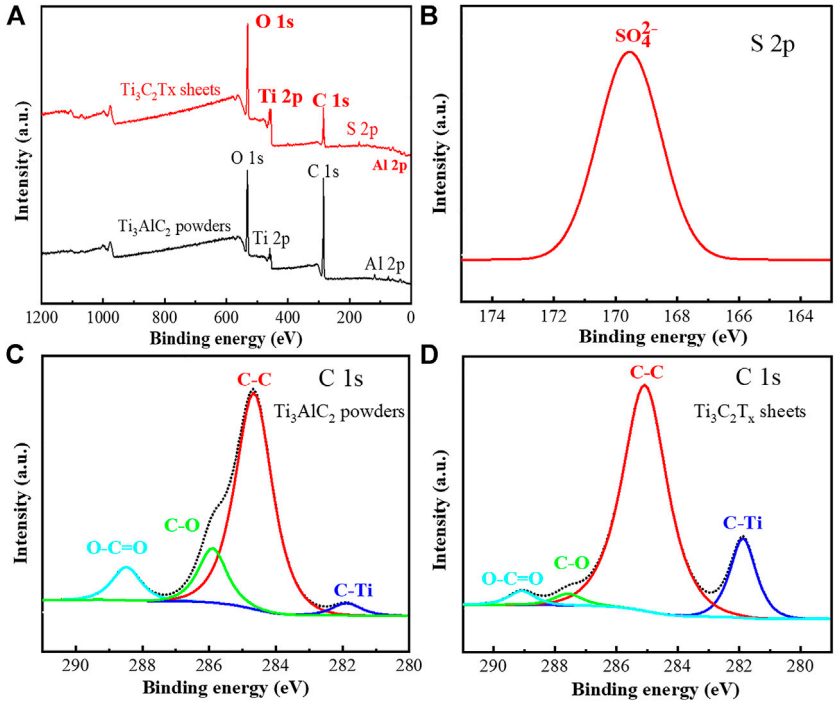

FIGURE 6
XPS survey spectra of Ti_3AlC_2 powders and $Ti_3C_2T_x$ sheets **(A)**, high-resolution S 2p XPS spectrum of $Ti_3C_2T_x$ sheets **(B)**, high-resolution C 1s XPS spectra of Ti_3AlC_2 powders and $Ti_3C_2T_x$ sheets, respectively **(C)** and **(D)**.

analysis (Figure 5B). As shown in Figures 6C,D, the characteristic C 1s peaks of the Ti_3AlC_2 powders and $Ti_3C_2T_x$ sheets also match those of previous work (Chen et al., 2020; Mathis et al., 2021), and the content ratio of C–Ti in the $Ti_3C_2T_x$ sheets is higher than that of Ti_3AlC_2 powders, suggesting that most of Al atomic layers in $Ti_3C_2T_x$ sheets have been selectively stripped.

The high-resolution Ti 2p XPS spectra of Ti_3AlC_2 powders and $Ti_3C_2T_x$ sheets show three characteristic peaks, corresponding to the Ti-C $2p_{3/2}$, Ti-C $2p_{1/2}$, and Ti-O orbitals, respectively (Figures 7A,B), consistent with the current literature reports (Li et al., 2019; Chen et al., 2020; Mathis et al., 2021). Moreover, based on the analysis of XPS data, the content of Ti increases from 5.50 At% of Ti_3AlC_2 powders to 10.50 At% of $Ti_3C_2T_x$ sheets.

On the other hand, the high-resolution Al 2p XPS spectra of Ti_3AlC_2 powders and $Ti_3C_2T_x$ sheets show three characteristic

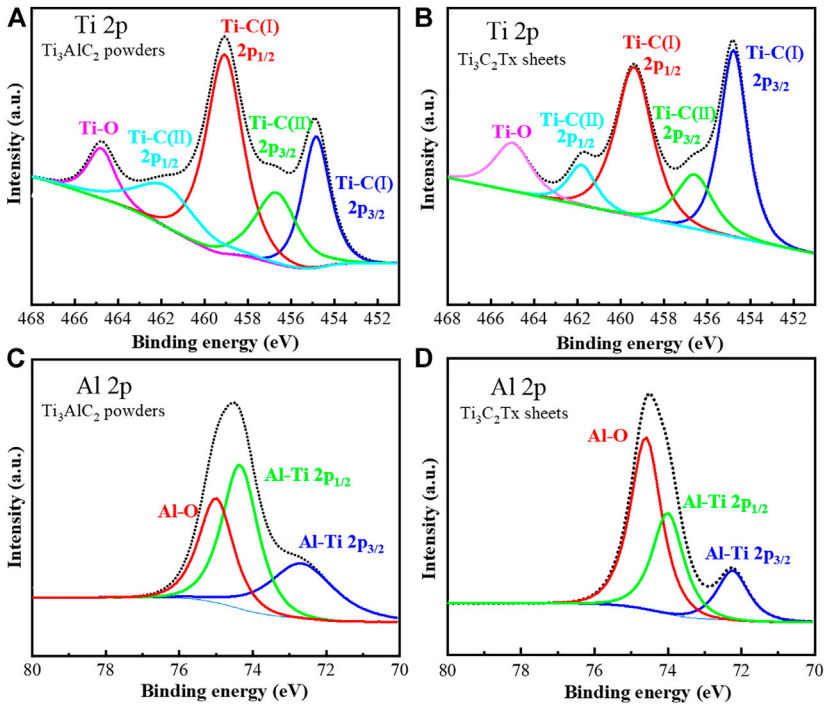

FIGURE 7
High-resolution XPS spectra of Ti 2p **(A)** and **(B)** and Al 2p **(C)** and **(D)** of Ti_3AlC_2 powders and $Ti_3C_2T_x$ sheets, respectively.

peaks (Chen et al., 2020; Mathis et al., 2021) corresponding to the Al-Ti $2p_{3/2}$, Al-Ti $2p_{1/2}$, and Al-O orbitals, respectively (Figures 7C,D). In particular, the content ratio of Al-Ti $2p_{3/2}$ and Al-Ti $2p_{1/2}$ in the $Ti_3C_2T_x$ sheets is significantly lower than that of Ti_3AlC_2 powders; in contrast, the content ratio of Al-O is higher. Based on the XPS analysis, the content of Al decreases from 6.50 At% of Ti_3AlC_2 powders to 1.50 At% of $Ti_3C_2T_x$ sheets. Thus, from the abovementioned content changes of Ti and Al on the XPS analysis before and after corrosion, it can be reasoned that most of the Al layers can be etched out; as a result, the atomic percentage of Al decreases, and the atomic percentage of Ti increases in the $Ti_3C_2T_x$ sheets.

Mechanism analysis

To analyze the selective etching process, some important factors should be considered as follows:

1) In the system of H_2SO_4 and H_2O_2, the aqueous solution H_2SO_4 of 6 mol/L is a strongly acidic medium with no volatility and 30% H_2O_2 acts as a strong green oxidizer without harmful by-products.
2) As the temperature is an important factor for the chemical reaction, to speed up the etching process, the temperature of the obtained mixture is heated by a temperature-controlled

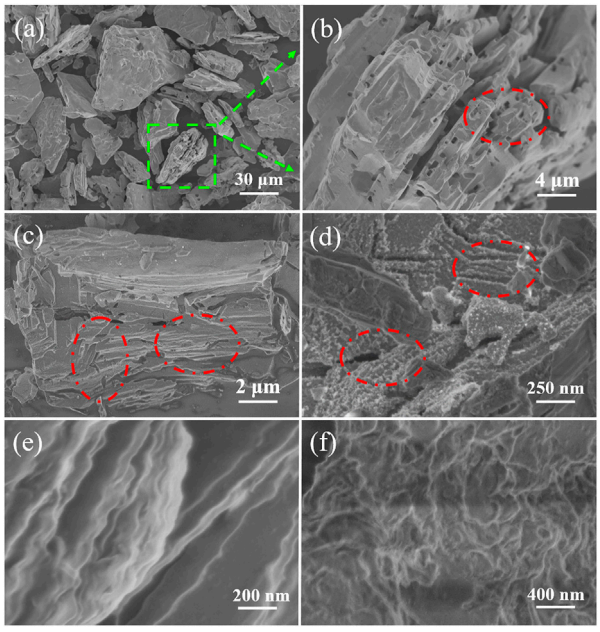

FIGURE 8
SEM images of intermediate sheets obtained by etching Ti_3AlC_2 powders in the H_2SO_4/H_2O_2 solution with different magnifications **(A–D)**, and SEM images of $Ti_3C_2T_x$ nanosheets with different magnifications **(E–F)**.

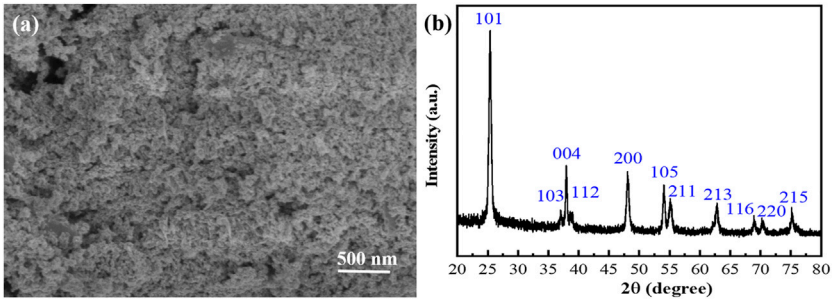

FIGURE 9
SEM image **(A)** and XRD patterns **(B)** of Al_2O_3 and TiO_2 nanocomposite.

water pot. In our experiment, if the temperature is too high, it will accelerate the decomposition of H_2O_2, and 40°C is chosen as the appropriate temperature. Moreover, no notable reaction occurs when the Ti_3AlC_2 powders are only mixed with an H_2SO_4 solution of 6 mol/L, and it is reasoned that the oxidant of H_2O_2 plays a major role in the etching process. Particularly, the content of H_2O_2 is very crucial for the etching process; if the oxidant of H_2O_2 is excessive, there will be some TiO_2 nanoparticles on the surface and interspace of MXene sheets because Ti can be oxidized to TiO_2 by excessive H_2O_2 (Huang et al., 2022; Ma et al., 2022). Otherwise, a certain amount of Ti_3AlC_2 is still present in $Ti_3C_2T_x$ without corrosion.

3) In the etching process, the microstructure change of intermediate sheets should be analyzed in detail. Seen from SEM images in Figures 8A,B, the obtained intermediate sheets show a loose, layered, and porous structure compared with Ti_3AlC_2 powders. This structure can be clearly demonstrated by the magnified parts of the selected area of the intermediate sheets (Figure 8B). Moreover, Figures 8C,D further reveal that the intermediate sheets are exfoliated along different directions, and lots of traces after stripping are left on the surface such as crack structures along longitudinal/transverse direction and TiO_2 nanoparticles on the surface (marked in the red circle of Figure 8D). Thus, the obtained $Ti_3C_2T_x$ nanosheets with clear layered and folded structures can be easily prepared after the intermediate sheets are stripped apart under ultrasonic treatment in deionized water (Figures 8E,F).

Moreover, the Al_2O_3 and TiO_2 nanocomposite (Figure 9A) can be obtained from the supernatant by adding a certain amount of NaOH solution, vacuum filtration, and drying. The precipitate of Al_2O_3 and TiO_2 can be precipitated by only adding an alkaline solution, which suggests that Al^{3+} ions accompanied by a small amount of TiO_2 are in the supernatant. As shown in Figure 9B, the XRD patterns of this nanocomposite are analyzed to prove the existence of Al_2O_3 and TiO_2 nanoparticles, consistent with those reported in the literature (Han et al., 2012; Abazari et al., 2014; Ali et al., 2018).

In summary, the relevant etching mechanism is may be attributed to the synergy effect of H_2SO_4 and H_2O_2, which triggers Al layers to be etched sequentially from the MAX phase. It is speculated that the reactive oxygen species (such as $HO^{\bullet}$ and $O_2^{\bullet-}$) radicals can be produced because H_2O_2 is heated in the course of our experiment, very similar to the advanced oxidation process of the photo-Fenton reaction (Liang et al., 2022). Thus, the radicals can weaken the Ti–Al bonds and attack the defect sites of the external surfaces of MAX phases (Liu et al., 2020; Wei et al., 2021), and synchronously, Al layers are etched into Al^{3+} ions in the aqueous H_2SO_4 solution of 6 mol/L, and there is no accumulation of $Al(OH)_3$ in this strongly acidic solution to retard this etching process. In addition, a lot of bubbles (such as O_2 and H_2) are produced to promote this etching process. Therefore, the synergy effect of H_2SO_4 and H_2O_2 triggers sequential selective etching of Al layers from the Ti_3AlC_2 phase.

On the other hand, abundant oxygen-containing functional groups are attached to the intermediate sheets, and Ti can be oxidized to TiO_2 by excessive H_2O_2. Interestingly, the SO_4^{2-} ions can be also inserted into the obtained $Ti_3C_2T_x$ nanosheets and TiO_2 nanoparticles can be *in situ* loaded on the surface of the obtained MXene nanosheets. The structure and morphology of the obtained MXene nanosheets can be further optimized by selecting the appropriate process such as the reaction rate and content of H_2O_2.

Conclusion

In conclusion, we develop a simple, safe, and efficient method to prepare MXene ($Ti_3C_2T_x$) nanosheets by selective etching Ti_3AlC_2 powders in a system of H_2SO_4/H_2O_2 and subsequent ultrasonic stripping. The obtained $Ti_3C_2T_x$ nanosheets can be confirmed from the characterization analyses of SEM, TEM, XRD, FTIR, and XPS. Lots of oxygen-containing functional groups (–O, –OH) are supported on the MXene surface, the SO_4^{2-} ions are inserted into the layers of the MXene sheets, and even TiO_2 nanoparticles can be *in situ* loaded due to the

oxidation of excessive H_2O_2. In the system of H_2SO_4/H_2O_2, the aqueous H_2SO_4 solution of 6 mol/L is a strongly acidic medium, and 30% H_2O_2 acts as a strong green oxidizer. The relevant etching mechanism may be attributed to the synergy effect of H_2SO_4 and H_2O_2, which triggers Al layers to be etched sequentially from the MAX phase. Our group is further exploring the etching mechanism. This work can provide a new way to develop HF-free and large-scale synthesis of 2D layered MXenes for many practical applications.

Data availability statement

The original contributions presented in the study are included in the article/Supplementary Material; further inquiries can be directed to the corresponding authors.

Author contributions

ZT and SB are responsible for designing and completing experiments. HT and KC are responsible for the preparation and characterization of materials. QP and YW are responsible for the literature search and review. QZ put forward constructive suggestions on the revision of the manuscript.

Funding

This work was supported by the Program for the High-Level Talents Start-up Fund (PXY-BSQD2016010) and the National Cultivation Fund (PXY-PYJJ2017001) of Pingdingshan University, the Natural Science Foundation of China (11904092), and the Hunan Provincial Natural Science Foundation (2019JJ50028).

Conflict of interest

The authors declare that the research was conducted in the absence of any commercial or financial relationships that could be construed as a potential conflict of interest.

Publisher's note

All claims expressed in this article are solely those of the authors and do not necessarily represent those of their affiliated organizations, or those of the publisher, the editors, and the reviewers. Any product that may be evaluated in this article, or claim that may be made by its manufacturer, is not guaranteed or endorsed by the publisher.

References

Abazari, R., Mahjoub, A. R., and Sanati, S. (2014). A facile and efficient preparation of anatase titania nanoparticles in micelle nanoreactors: Morphology, structure, and their high photocatalytic activity under UV light illumination. *RSC Adv.* 4, 56406–56414. doi:10.1039/c4ra10018b

Alhabeb, M., Maleski, K., Anasori, B., Lelyukh, P., Clark, L., Sin, S., et al. (2017). Guidelines for synthesis and processing of two-dimensional Titanium carbide ($Ti_3C_2T_x$ MXene). *Chem. Mat.* 29, 7633–7644. doi:10.1021/acs.chemmater.7b02847

Alhabeb, M., Maleski, K., Mathis, T. S., Sarycheva, A., Hatter, C. B., Uzun, S., et al. (2018). Selective etching of Silicon from Ti_3SiC_2 (MAX) to obtain 2D Titanium carbide (MXene). *Angew. Chem. Int. Ed. Engl.* 57, 5542–5546. doi:10.1002/ange.201802232

Ali, A. S., Mohammed, A. J., and Saud, H. R. (2018). Hydrothermal synthesis of TiO2/Al2O3 nanocomposite and its application as improved sonocatalyst. *Int. J. Eng. Technol.* 7, 22–25. doi:10.14419/ijet.v7i4.37.23607

Anasori, B., Lukatskaya, M. R., and Gogotsi, Y. (2017). 2D metal carbides and nitrides (MXenes) for energy storage. *Nat. Rev. Mat.* 2, 16098. doi:10.1038/natrevmats.2016.98

Chen, W. Y., Jiang, X., Lai, S-N., Peroulis, D., and Stanciu, L. (2020). Nanohybrids of a MXene and transition metal dichalcogenide for selective detection of volatile organic compounds. *Nat. Commun.* 11, 1302. doi:10.1038/s41467-020-15092-4

Dillon, A. D., Ghidiu, M. J., Krick, A. L., Griggs, J., May, S. J., Gogotsi, Y., et al. (2016). Highly conductive optical quality solution-processed films of 2D Titanium carbide. *Adv. Funct. Mat.* 26, 4162–4168. doi:10.1002/adfm.201600357

Fan, Y., Li, L., Zhang, Y., Zhang, X., Geng, D., Hu, W., et al. (2022). Recent advances in growth of Transition metal carbides and nitrides (MXenes) crystals. *Adv. Funct. Mat.* 32, 2111357. doi:10.1002/adfm.202111357

Gao, X., Wang, B., Wang, K., Xu, S., Liu, S., Liu, X., et al. (2021). Design of Ti3C2Tx/TiO2/PANI multi-layer composites for excellent electromagnetic wave absorption performance. *J. Colloid Interface Sci.* 583, 510–521. doi:10.1016/j.jcis.2020.09.094

Ghazaly, A. E., Ahmed, H., Rezk, A. R., Halim, J., Persson, Per O. Å., Yeo, L. Y., et al. (2021). Ultrafast, one-step, salt-solution-based acoustic synthesis of Ti_3C_2 MXene. *ACS Nano* 15, 4287–4293. doi:10.1021/acsnano.0c07242

Ghidiu, M., Lukatskaya, M. R., Zhao, M. Q., Gogotsi, Y., and Barsoum, M. W. (2014). Conductive two-dimensional Titanium carbide'clay' with high volumetric capacitance. *Nature* 516, 78–81. doi:10.1038/nature13970

Gogotsi, Y., and Anasori, B. (2019). The rise of MXenes. *ACS Nano* 13, 8491–8494. doi:10.1021/acsnano.9b06394

Halim, J., Lukatskaya, M. R., Cook, K. M., Lu, J., Smith, C. R., Naslund, L. A., et al. (2014). Transparent conductive two-dimensional Titanium carbide epitaxial thin films. *Chem. Mat.* 26, 2374–2381. doi:10.1021/cm500641a

Han, C., Luque, R., and Dionysiou, D. D. (2012). Facile preparation of controllable size monodisperse anatase titania nanoparticles. *Chem. Commun.* 48, 1860–1862. doi:10.1039/c1cc16050h

Hantanasirisakul, K., Zhao, M. Q., Urbankowski, P., Halim, J., Anasori, B., Kota, S., et al. (2016). Fabrication of $Ti_3C_2T_x$ MXene transparent thin films with tunable optoelectronic properties. *Adv. Electron. Mat.* 2, 1600050. doi:10.1002/aelm.201600050

Huang, Y., Lu, Q., Wu, D., Jiang, Y., Liu, Z., Chen, B., et al. (2022). Flexible MXene films for batteries and beyond. *Carbon Energy* 4, 598–620. doi:10.1002/cey2.200

Iqbal, A., Shahzad, F., Hantanasirisakul, K., Kim, M-K., Kwon, J., Hong, J., et al. (2020). Anomalous absorption of electromagnetic waves by 2D transition metal carbonitride Ti_3CNT_x (MXene). *Science* 369, 446–450. doi:10.1126/science.aba7977

Jawaid, A., Hassan, A., Neher, G., Nepal, D., Pachter, R., Kennedy, W. J., et al. (2021). Halogen etch of Ti_3AlC_2 MAX phase for MXene fabrication. *ACS Nano* 15, 2771–2777. doi:10.1021/acsnano.0c08630

Jiang, J., Bai, S., Zou, J., Liu, S., Hsu, J-P., Li, N., et al. (2022). Improving stability of MXenes. *Nano Res.* 15, 6551–6567. doi:10.1007/s12274-022-4312-8

Li, G., Tan, L., Zhang, Y., Wu, B., and Li, L. (2017). Highly efficiently delaminated single-layered MXene nanosheets with large lateral size. *Langmuir* 33, 9000–9006. doi:10.1021/acs.langmuir.7b01339

Li, M., Lu, J., Luo, K., Li, Y., Chang, K., Chen, K., et al. (2019). Element replacement approach by reaction with Lewis acidic molten salts to synthesize nanolaminated MAX phases and MXenes. *J. Am. Chem. Soc.* 141, 4730–4737. doi:10.1021/jacs.9b00574

Li, T., Yao, L., Liu, Q., Gu, J., Luo, R., Li, J., et al. (2018). Fluorine-free synthesis of high-purity $Ti_3C_2T_x$ (T= OH, O) *via* alkali treatment. *Angew. Chem. Int. Ed.* 57, 6115–6119. doi:10.1002/anie.201800887

Liang, L., Niu, L., Wu, T., Zhou, D., and Xiao, Z. (2022). Fluorine-free fabrication of MXene *via* photo-Fenton approach for advanced lithium-sulfur batteries. *ACS Nano* 16, 7971–7981. doi:10.1021/acsnano.2c00779

Liang, X., Garsuch, A., and Nazar, L. F. (2015). Sulfur cathodes based on conductive MXene nanosheets for high-performance lithium-sulfur batteries. *Angew. Chem. Int. Ed. Engl.* 54, 3979–3983. doi:10.1002/ange.201410174

Lin, X. H. (2015). Impact of the spatial distribution of sulfate species on the activities of SO42−/TiO2 photocatalysts for the degradation of organic pollutants in reverse osmosis concentrate. *Appl. Catal. B Environ.* 170, 263–272. doi:10.1016/j.apcatb.2015.02.001

Liu, A., Liang, X., Ren, X., Guan, W., Gao, M., Yang, Y., et al. (2020). Recent progress in MXene-based materials: Potential high-performance electrocatalysts. *Adv. Funct. Mat.* 30, 2003437. doi:10.1002/adfm.202003437

Lukatskaya, M. R., Mashtalir, O., Ren, C. E., Dall'Agnese, Y., Rozier, P., Taberna, P. L., et al. (2013). Cation intercalation and high volumetric capacitance of two-dimensional Titanium carbide. *Science* 341, 1502–1505. doi:10.1126/science.1241488

Luo, J., Matios, E., Wang, H., Tao, X., and Li, W. (2020). Interfacial structure design of MXene-based nanomaterials for electrochemical energy storage and conversion. *InfoMat* 2, 1057–1076. doi:10.1002/inf2.12118

Ma, Y., Cheng, Y., Wang, J., Fu, S., Zhou, M., Yang, Y., et al. (2022). Flexible and highly-sensitive pressure sensor based on controllably oxidized MXene. *InfoMat* 4, e12328. doi:10.1002/inf2.12328

Mashtalir, O., Naguib, M., Mochalin, V. N., Dall'Agnese, Y., Heon, M., Barsoum, M. W., et al. (2013). Intercalation and delamination of layered carbides and carbonitrides. *Nat. Commun.* 4, 1716. doi:10.1038/ncomms2664

Mathis, T. S., Maleski, K., Goad, A., Sarycheva, A., Anayee, M., Foucher, A. C., et al. (2021). Modified MAX phase synthesis for environmentally stable and highly conductive Ti3C2 MXene. *ACS Nano* 15, 6420–6429. doi:10.1021/acsnano.0c08357

Naguib, M., Barsoum, M. W., and Gogotsi, Y. (2021). Ten years of progress in the synthesis and development of MXenes. *Adv. Mat.* 2021, 2103393. doi:10.1002/adma.202103393

Naguib, M., and Gogotsi, Y. (2015). Synthesis of two-dimensional materials by selective extraction. *Acc. Chem. Res.* 48, 128–135. doi:10.1021/ar500346b

Naguib, M., Kurtoglu, M., Presser, V., Lu, J., Niu, J., Heon, M., et al. (2011). Two-dimensional nanocrystals produced by exfoliation of Ti_3AlC_2. *Adv. Mat.* 23, 4248–4253. doi:10.1002/adma.201102306

Pang, S-Y., Wong, Y-T., Yuan, S., Liu, Y., Tsang, M-K., Yang, Z., et al. (2019). Universal strategy for HF-free facile and rapid synthesis of two-dimensional MXenes as multifunctional energy materials. *J. Am. Chem. Soc.* 141, 9610–9616. doi:10.1021/jacs.9b02578

Park, K. W., and Leitao, E. M. (2021). The link to polysulfides and their applications. *Chem. Commun.* 57, 3190–3202. doi:10.1039/d1cc00505g

Ren, C. E., Hatzell, K. B., Alhabeb, M., Ling, Z., Mahmoud, K. A., and Gogotsi, Y. (2015). Charge- and size-selective ion sieving through $Ti_3C_2T_x$ MXene membranes. *J. Phys. Chem. Lett.* 6, 4026–4031. doi:10.1021/acs.jpclett.5b01895

Sang, X., Xie, Y., Lin, M. W., Alhabeb, M., Van Aken, K. L., Gogotsi, Y., et al. (2016). Atomic defects in monolayer Titanium carbide ($Ti_3C_2T_x$) MXene. *ACS Nano* 10, 9193–9200. doi:10.1021/acsnano.6b05240

Seh, Z. W., Fredrickson, K. D., Anasori, B., Kibsgaard, J., Strickler, A. L., Lukatskaya, M. R., et al. (2016). Two-dimensional Molybdenum carbide (MXene) as an efficient electrocatalyst for hydrogen evolution. *ACS Energy Lett.* 1, 589–594. doi:10.1021/acsenergylett.6b00247

Shahzad, F., Alhabeb, M., Hatter, C. B., Anasori, B., Man Hong, S., Koo, C. M., et al. (2016). Electromagnetic interference shielding with 2D transition metal carbides (MXenes). *Science* 353, 1137–1140. doi:10.1126/science.aag2421

Shi, H., Zhang, P., Liu, Z., Park, S. W., Lohe, M. R., Wu, Y., et al. (2021). Ambient-stable two-dimensional Titanium carbide (MXene) enabled by Iodine etching. *Angew. Chem. Int. Ed. Engl.* 60, 8771–8775. doi:10.1002/ange.202015627

Shi, L-N., Cui, L-T., Ji, Y-R., Xie, Y., Zhu, Y-R., and Yi, T-F. (2022). Towards high-performance electrocatalysts: Activity optimization strategy of 2D MXenes-based nanomaterials for water-splitting. *Coord. Chem. Rev.* 469, 214668. doi:10.1016/j.ccr.2022.214668

Shi, Y., Zhou, D., Wu, T., and Xiao, Z. (2022). Deciphering the $Sb_4O_5Cl_2$-MXene hybrid as a potential anode material for advanced potassium-ion batteries. *ACS Appl. Mat. Interfaces* 14, 29905–29915. doi:10.1021/acsami.2c06948

Shuck, C. E., Sarycheva, A., Anayee, M., Levitt, A., Zhu, Y., Uzun, S., et al. (2020). Scalable synthesis of Ti_3C_2Tx MXene. *Adv. Eng. Mat.* 2020, 1901241. doi:10.1002/adem.201901241

Tao, Q., Dahlqvist, M., Lu, J., Kota, S., Meshkian, R., Halim, J., et al. (2017). Two-dimensional $Mo_{1.33}C$ MXene with divacancy ordering prepared from parent 3D laminate with in-plane chemical ordering. *Nat. Commun.* 8, 14949. doi:10.1038/ncomms14949

VahidMohammadi, A., Rosen, J., and Gogotsi, Y. (2021). The world of two-dimensional carbides and nitrides (MXenes). *Science* 372, eabf1581. doi:10.1126/science.abf1581

Wang, C., Shou, H., Chen, S., Wei, S., Lin, Y., Zhang, P., et al. (2021). HCl-based hydrothermal etching strategy toward fluoride-free MXenes. *Adv. Mat.* 33, 2101015. doi:10.1002/adma.202101015

Wang, X., Kajiyama, S., Iinuma, H., Hosono, E., Oro, S., Moriguchi, I., et al. (2015). Pseudocapacitance of MXene nanosheets for high-power sodium-ion hybrid capacitors. *Nat. Commun.* 6, 6544. doi:10.1038/ncomms7544

Wang, Z., Xuan, J., Zhao, Z., Li, Q., and Geng, F. (2017). Versatile cutting method for producing fluorescent ultrasmall MXene sheets. *ACS Nano* 11, 11559–11565. doi:10.1021/acsnano.7b06476

Wei, Y., Zhang, P., Soomro, R. A., Zhu, Q., and Xu, B. (2021). Advances in the synthesis of 2D MXenes. *Adv. Mat.* 2021, 2103148. doi:10.1002/adma.202103148

Xu, M., Liang, L., Qi, J., Wu, T., Zhou, D., and Xiao, Z. (2021). Intralayered ostwald ripening-induced self-catalyzed growth of CNTs on MXene for robust lithium–sulfur batteries. *Small* 17, 2007446. doi:10.1002/smll.202007446

Xu, M., Wu, T., Qi, J., Zhou, D., and Xiao, Z. (2021). V_2C/VO_2 nanoribbon intertwined nanosheet dual heterostructure for highly flexible and robust lithium-sulfur batteries. *J. Mat. Chem. A* 9, 21429–21439. doi:10.1039/d1ta05693j

Xu, M., Zhou, D., Wu, T., Qi, J., Du, Q., and Xiao, Z. (2022). Self-regulation of spin polarization density propelling the ion diffusion kinetics for flexible potassium-ion batteries. *Adv. Funct. Mat.* 2022, 2203263. doi:10.1002/adfm.202203263

Zhang, M., Yang, D., Dong, C., Huang, H., Feng, G., Chen, Q., et al. (2022). Two-dimensional MXene-originated *in situ* nanosonosensitizer generation for augmented and synergistic sonodynamic tumor nanotherapy. *ACS Nano* 16, 9938–9952. doi:10.1021/acsnano.2c04630

Zhou, J., Zha, X., Zhou, X., Chen, F., Gao, G., Wang, S., et al. (2017). Synthesis and electrochemical properties of two-dimensional Hafnium carbide. *ACS Nano* 11, 3841–3850. doi:10.1021/acsnano.7b00030